International Journal of Earth Sciences

The use of HVSR measurements for investigating buried tectonic structures: the Mirandola Anticline, northern Italy, as a case study

--Manuscript Draft--

Manuscript Number:	
Full Title:	The use of HVSR measurements for investigating buried tectonic structures: the Mirandola Anticline, northern Italy, as a case study
Article Type:	Original Paper
Keywords:	seismic hazard; seimotectonics; single station microtremor; HVSR; blind anticline; Po Plain.
Corresponding Author:	Gabriele Tarabusi Istituto Nazionale di Geofisica e Vulcanologia ITALY
Corresponding Author Secondary Information:	
Corresponding Author's Institution:	Istituto Nazionale di Geofisica e Vulcanologia
Corresponding Author's Secondary Institution:	
First Author:	Gabriele Tarabusi
First Author Secondary Information:	
Order of Authors:	Gabriele Tarabusi
	Riccardo Caputo
Order of Authors Secondary Information:	
Funding Information:	
Abstract:	The Mirandola Anticline represents a buried fault-propagation fold which has been growing during Quaternary due to the seismogenic activity of a blind segment belonging to the broader Ferrara Arc. The last reactivation occurred during the May 2012 Emilia sequence. In correspondence with this structure the thickness of the marine and continental deposits of the Po Plain foredeep is particularly reduced. In order to better define the shallow geometry of this tectonic structure, and hence its recent activity, we investigated in a depth range which is intermediate between the surficial morphological observations and seismic profiles information. In particular, we carried out numerous passive seismic measurements (single station microtremor) for obtaining the horizontal to vertical spectral ratio (HVSR). The results of a combined analysis of the peak frequency and its amplitude nicely fit the available geological information suggesting that this low-cost geophysical technique could be successfully applied in other sectors of wide morphologically flat alluvial plains to investigate blind and completely buried potential seismogenic structures.

The use of HVSR measurements for investigating buried tectonic structures: the Mirandola Anticline, northern Italy, as a case study

Tarabusi G.[1,2] (gabriele.tarabusi@ingv.it, +393284597003) and Caputo R.[1,3]

1) Dept. of Physics and Earth Sciences, Ferrara University, via Saragat 1, 44122 Ferrara, Italy

2) Istituto Nazionale di Geofisica e Vulcanologia, via di vigna murata 605, 00143 Roma, Italy

3) Research and Teaching Center for Earthquake Geology, Tyrnavos, Greece

Abstract

The Mirandola Anticline represents a buried fault-propagation fold which has been growing during Quaternary due to the seismogenic activity of a blind segment belonging to the broader Ferrara Arc. The last reactivation occurred during the May 2012 Emilia sequence. In correspondence with this structure the thickness of the marine and continental deposits of the Po Plain foredeep is particularly reduced. In order to better define the shallow geometry of this tectonic structure, and hence its recent activity, we investigated in a depth range which is intermediate between the surficial morphological observations and seismic profiles information. In particular, we carried out numerous passive seismic measurements (single station microtremor) for obtaining the horizontal to vertical spectral ratio (HVSR). The results of a combined analysis of the peak frequency and its amplitude nicely fit the available geological information suggesting that this low-cost geophysical technique could be successfully applied in other sectors of wide morphologically flat alluvial plains to investigate blind and completely buried potential seismogenic structures.

keywords: seismic hazard; seimotectonics; single station microtremor; HVSR; blind anticline; Po Plain.

Introduction

In May 2012, two moderate (M_L = 5.9 and 5.8 or Mw = 6.1 and 5.9; *e.g.* Pondrelli *et al.* 2012) earthquakes, associated with a noticeable aftershock sequence (*e.g.* Saraò and Peruzza 2012; Scognamiglio *et al.*, 2012), affected the eastern sector of the Po Plain, Italy. The causative faults are two segments of the Ferrara Arc thrust system representing the most frontal portion of the buried Northern Apennines fold-and-thrust belt (*e.g.* Vannoli *et al.* 2015; Figure 1). In particular, the two major structures which were reactivated have a left-stepping largely overlapping geometry. Both seismogenic sources were associated with blind, mainly dip-slip reverse, faulting (*e.g.* Scognamiglio *et al.* 2012; Pondrelli *et al.* 2012), while the uppermost tip segment of the sliding planes has been estimated to reach a minimum depth of 3-4 km (Bignami *et al.* 2012). As a consequence of the fault geometry and kinematics, the rock volume above the co-seismic rupture tip was characterised by a typical fault-propagation folding process that eventually caused the bending of the topographic surface and the consequent uplift of the broader epicentral area (Bignami *et al.* 2012; Salvi *et al.* 2012; Caputo *et al.* 2015).

However during the long interseismic periods, the high sedimentation rate characterizing the Po Plain tends to compensate the seismically induced topographic variations. The repeating of similar 'areal morphogenic earthquakes' (Caputo 2005) during Late Pleistocene and Holocene locally caused cumulative effects in the coeval stratigraphic succession. Although such stratigraphic lateral variations are relatively evident in the deeper geology (Pieri and Groppi 1981; Boccaletti *et al.* 2004), they are morphologically subtle in the otherwise flat topography of the alluvial plain and they could be emphasized only by a careful inspection of the hydrographic network, which indeed highlights the occurrence of several drainage anomalies (*e.g.* Burrato *et al.* 2003; 2012). Such hydrographic anomalies were considered key features for documenting the recent tectonic activity of the underlying faults (Basili *et al.* 2008; DISS WG 2015) whose instrumental or even historical seismic record is relatively poor likely due to the long recurrence intervals on these structures.

In the present paper we focus on the shallow subsoil, say the first 100-200 m, representing an intermediate-depth investigation target between the deep geological elements and the surface features. The former could be only observed based on very expensive seismic reflection profiles generally carried out for hydrocarbon purposes; however, these geophysical surveys are not always available, but above all the details for the uppermost stratigraphic levels are commonly not sufficient to document the most recent tectonic activity of blind thrusts. Indeed, due to the deeper target of such explorations, the analysis of the uppermost sediments, which could potentially record a recent seismogenic activity, are often deliberately neglected since the preliminary planning phases of the geophysical survey.

On the other hand, the cumulative effects of coseismically induced surface deformations could be only emphasized and recognized on the basis of very detailed topographic, hydrographic and morphological analyses (*e.g.* Burrato *et al.* 2003; 2012). Also in this case, however, the effects of anthropogenic manipulations and the fluvial dynamics occurring during the long interseismic periods, commonly in the order of thousands of years, often hinder the doubtless identification of the seismogenic behaviour associated with a recognized underlying fault.

The occasion of starting this scientific project was the preparation of a seismic microzonation map for the Municipality of Mirandola, Emilia-Romagna (Northern Italy). This work was financially supported by the Municipality and the Italian Dipartimento di Protezione Civile in the frame of an agreement with the regional administrations (OPCM 3907/2010, DGR 1051/2011). It is noteworthy that this investigation was commissioned in winter 2011-2012 and the report complete of maps was released few months before the seismic sequence that affected the broader area (Tarabusi 2012).

For the aims of this paper, numerous passive seismic measurements (single station microtremor analyses) were performed in order to improve and especially enlarge the database originally collected for the microzonation study. Therefore, this work allowed to investigate a much wider area corresponding to a large part of the Mirandola anticline.

Methodology

The passive seismic measurements have been carried out using a digital tromograph (Tromino$^{(R)}$) that records the background noise in order to obtain the natural resonance frequencies within the underground. We followed the three general reliability conditions proposed in the SESAME user guidelines (Koller *et al.* 2004; Bard *et al.* 2005). Then natural resonance frequency has been also directly correlated with local seismic amplification which is commonly considered as the principal source of damage in case of earthquake shaking (*e.g.* Mucciarelli *et al.* 2001; Gallipoli *et al.* 2004). The background noise, also referred to as microtremor, is present everywhere at the Earth's surface and could be associated also with both atmospheric phenomena and anthropogenic activities. It is generally characterised by very small oscillations with spectral components poorly attenuated in space and measurable with passive recording techniques. All elastic waves during their path from the source to a site suffer some attenuation which is basically geometric, due to the increasing dimensions of the wave front, and anelastic, due to the real not perfectly elastic behaviour of all rocks. In both cases, the amount of attenuation is a function of frequency; indeed, assuming a constant velocity for all frequencies, the shorter the wavelength (*i.e.* the higher the frequency) the greater the number of cycles and hence of the attenuation occurred. Accordingly, stratigraphic layering governs the distribution of the mechanical properties (*e.g.* Castellaro *et al.* 2005). Such information is included in the recorded microtremors together with random noise, and it can be extracted by means of several methods like the one proposed by Nakamura (1989; horizontal to vertical spectral ratio, HVSR). This technique is nowadays largely used in order to determine the local seismic amplification and to estimate the principal resonance frequencies characterising the shallow subsoil, say from tens to few hundreds of meters. Both outcomes are crucial for engineering antiseismic planning.

The H/V method assumes the microtremors as mainly consisting of Rayleigh waves, both vertical and horizontal components, which are amplified as a consequence of site effects induced by the presence of stratigraphic discontinuities within the subsoil. Based on a Fourier transform, it is thus possible to reconstruct, in the frequency domain, the spectral distribution of both horizontal and vertical records (measured in the time domain) and hence calculate the HVSR. The occurrence of a peak in the HVSR curve documents the presence of a mechanical discontinuity along the vertical of the measured site.

The field work was carried out with three different instruments and several tests have been performed by repeating the measurements at a same site at different times for checking repeatibility of results. Sampling was at 128 Hz with recording times between 30 and 12 minutes according to the SESAME criteria (Koller *et al.* 2004; Bard *et al.* 2005) for a reliable H/V curve. The Grilla software (Micromed. 2006; 2008) was used for elaborating the records within the frequency interval 0-64 Hz, considering time windows of 20 s and a smoothing technique based on a 10% wide triangular window.

Natural frequencies and amplitudes

Within a strongly subsiding foredeep basin, like the Po Plain since Middle Pleistocene, in correspondence with the structural culminations of the fault-propagation anticlines, the thickness of the continental Quaternary deposits is generally reduced. Moreover, these deposits generally consist of condensed sedimentary successions or even temporal *hiatuses*, and in this region they directly overlay the Pliocene marine units (Pieri and Groppi 1981; Boccaletti *et al.* 2004; Martelli and Molinari 2008). As a consequence, a high impedance contrast occurs due to the abrupt increase of both seismic waves velocity and material density. Accordingly, these mechanical conditions are favourable to be detected on the basisd of HVSR analyses.

In particular, when the lithological change is sharp and stratigraphically reduced to (less than) few meters, a high and marked amplification peak is expected to form in the HVSR curve. As commonly accepted in the literature, the frequency of the amplification peak is at a first approximation proportional to the shear wave velocity of the overlying sedimentary body and to the inverse of the discontinuity depth according to the formula (the so called resonance equation)

$$f_0 = \frac{v_s}{4 \cdot h} \qquad [1]$$

In some sectors of the buried anticlines, a relatively thin layer of Upper Pliocene-Lower Pleistocene marine deposits (even just 20-30 m) could be interposed between the overlying 'condensed' continental sedimentary succession and the underlying lithological units. In this geological setting, the impedance contrast is somehow distributed or possibly splitted between more than one surface. In this case, the HVSR analysis shows two (or more) very close peaks or a relatively wide one (Oliveto *et al.* 2004; Castellaro *et al.* 2005).

In principle, the higher the peak, the greater the impedance contrast between the two layers, while the narrower the peak (*i.e.* characterized by a very small range of frequencies), the sharper is the lithological variation in the stratigraphic column.

Areal distribution

During the geophysical campaigns a total number of about 150 measurements have been performed. About 10% of them where discarded according to the SESAME criteria and based on the single component Fourier spectra, or because affected by anthropogenic disturbances. Accordingly, only 136 measurements have been further considered and subsequently analysed for the purpose of this paper (Table 1). They are distributed all over the investigated area (Figure 2), though with a variable density in order to better highlight the geometry of the Mirandola anticline, which represents the structural and stratigraphic case study investigated in this paper. As above mentioned, for each site the amplitude of the peak value of the HVSR curve, *A*, and the corresponding frequency, f_0 (commonly referred to as *natural frequency*), have been considered (an example is shown in Figure 3). At this regard it should be noted that only the peaks between 0.2-0.4 and ~10 Hz have been analysed. Indeed, peaks at lower frequencies could be possibly influenced by the meteorological conditions (Castellaro and Mulargia 2007), while peaks at f_0 > 10 Hz are associated with very shallow stratigraphic reflectors of no interest for the purpose of this paper.

The distribution of both parameters has been further elaborated by creating a colour-shaded map using the kriging interpolation method included in Golden Software Surfer(R). The results of the geophysical campaign and the gridding clearly document the presence of areas characterized by resonance phenomena, locally very important ones, and allow to map their distribution. In particular, Figure 4 evidences the occurrence of a narrow zone (2.5-3.5 km-wide), trending ESE-WNW and characterized by *A* values of the HVSR curves (Figure 3) greater than 2,5. Local maxima occur, from west to east, along the central sector.

A similar pattern could be also observed in Figure 5, where the natural frequency f_0 has been interpolated with the same procedure described above. In this case, the selected discriminant value is *ca.* 1 Hz and the gridding emphasizes an elongated ESE-WNW trending area characterized by natural frequencies up to 2.0 Hz. Assuming as a first approximation laterally uniform (or smoothly variable) seismic waves velocities within the uppermost sedimentary units, say the first 100-150 m, the mapped distribution of the natural frequencies is certainly due to a strongly variable depth of the surface producing the resonance (*i.e.* characterized by an impedance contrast).

The areas emphasized in Figures 4 and 5 basically coincide and are both characterized by marked gradients north and south and a progressive fading ESE-wards. Position and dimensions of the overlapping area as well as the corresponding values of the two mapped parameters are due to laterally changing impedance contrast associated with the variable stratigraphic succession developed during Pliocene-Quaternary on top of the Mirandola anticline.

Interface depth

A geological cross section based on seismic reflection profiles (Martelli and Molinari 2008) and realized for investigating possible geothermal reservoirs in the area of Mirandola is represented for reference in Figure 6b. On top of the profile are also plotted the HVSR curves obtained from sites measured within a distance of *ca.* 200 m from the trace of the geological section (A-A' in Figure 2). Accordingly, we tentatively correlated laterally the major peaks and few secondary ones in order to obtain a pseudo-2D section representing the principal surfaces characterized by impedance contrast. As it could be clearly observed, there is a good agreement between the reconstructed subsoil geometry of the Pliocene and Quaternary sedimentary bodies and the position (*i.e.* frequency) and shape of the peaks in the different HVSR curves (Figure 6a). In particular, in correspondence of the top of the Mirandola anticline, the HVSR curves show a marked peak, locally as high as 5.8, progressively decreasing in amplitude *A* both northwards and southwards, that is to say moving toward the two contiguous synclines. From a mechanical and hence seismological point of view, these HVSR variations (Figure 6a) could be due to a laterally variable impedance contrast particularly related to an impedance increase of the sedimentary body below the interface in correspondence of the anticline. This could be a consequence of i) differential compaction, ii) the direct contact with older (*i.e.* more compacted and denser) layers following the partial erosion of the upper part of the underlying succession and/or iii) a condensed overlying sedimentary series. Following the same approach, we also attempted to correlate other secondary peaks (Figure 6a), which emphasize the pinch-out geometry of the sedimentary bodies infilling the synclines both north and south of the Mirandola anticline.

Discussion

It is worth to note that the overall picture of the buried Mirandola anticline has been obtained in this paper based only on the large number of single station measurements that allowed to laterally correlate the peak frequency and amplitude of the HVSR curves and especially to give a stratigraphic meaning to the interfaces corresponding to the observed peaks (Figures 4 and 5).

In order to further constrain and validate the subsoil model here proposed, we also carried out HVSR measurements in correspondence of two boreholes cored by Regione Emilia-Romagna down to a depth of 101 and 127 m, respectively (see Figure 2 for location). Accordingly, at these two sites the detailed stratigraphic succession has been reconstructed showing the occurrence of the Pliocene Top, the so called seismic pseudo-bedrock interface of the area (*i.e.* $v_s \geq 600$ m/s). at *ca.* 95 and 116 m, respectively (Luca Martelli, pers. comm.). Moreover, at both sites a second borehole was drilled to perform a crosshole investigation for measuring the velocity distribution at depth (Figures 7a,b). Based on a simplified inversion approach (Castellaro and Mulargia 2009), we succeeded to reproduce our measured HVSR curves and particularly the major and meaningful peaks down to the bedrock interface separating the continental Middle Quaternary from the marine Early Quaternary-Late Pliocene deposits (Figures 7c,d). The slight misfit with increasing depth is possibly due to the progressive loss of verticality and hence of parallelism between the two boreholes used for the crosshole measurements that could have introduced a velocity error in the deeper part of the borehole measurement.

Additionally, based on the inversion of the H/V curves where independent geotechnical or other geophysical data are available (Castellaro and Mulargia 2009), it was also possible to calculate for selected sites the shear waves velocity in the first 30 m (v_{s30}) and down to the bedrock (v_{sH}, where H represents a depth between 75 and ca. 150 m in correspondence with the anticline). Both seismic parameters are particularly important for better evaluating the amplification factor by following the so called simplified procedures commonly used, for example, in Italian microzonation investigations (Gruppo di lavoro MS 2008; Regione Emilia-Romagna 2007).

Following the resonance equation [1], a good estimate of the shear-waves velocity of the deposits overlying the lithological discontinuity could allow to constrain its depth. The estimated values of the v_{s30} and especially of the v_{sH} vary from 190 to 220 m/s and from 290 to 320 m/s, respectively, at the two measured sites of Medolla and Mirandola (Figures 7a,b). Accordingly, the inferred depth of the recognized discontinuity emphasized by the natural frequency distribution (Figure 5) ranges between 75-90 m, on the crest of the Mirandola anticline (*e.g.* near San Giacomo in Roncole; Figure 2), to more than 150 m both north and south along the two flanks of the fold and towards the eastern pericline (the investigated area does not cover the western termination of the buried tectonic structure).

Although in laterally heterogeneous sedimentary successions a much larger number of boreholes would be necessary to establish a reliable frequency-thickness relationships (*e.g.* Ibs von Seht and Wohlenberg 1999; Gosar and Lenart 2010), our investigated area is characterized by a smoothly variable stratigraphy and hence we consider the calibration performed at the two boreholes of Regione Emilia-Romagna as sufficiently constrained for the purpose of this paper.

According to the calibrated mean velocity profiles and following the same approach previously described and used for laterally correlating 1D HVSR measurements (Figure 6a), we elaborated several transects oriented NNE-SSW, that are running across the buried anticline (traces *a* to *g* in Figure 2). The results of this approach and the tentative correlations among the different HVSR peaks are shown in Figure 8, where it is possible to observe a substantially uniform pattern marked by some major surfaces (*i.e.* characterised by impedance contrast) converging both north and south towards the top of the anticline. This geometry is emphasized by the more pronounced and relatively higher frequency peaks, which commonly correspond to the shallowest depth of the so called seismic pseudo-bedrock (*i.e.* $v_s \geq 600$ m/s).

Concluding remarks

Seismic amplification is influenced by the stiffness of the soil, and especially by the impedance contrast among shallow seismic units. Accordingly, maps of natural frequency are of utmost importance because they allow to recognize areas characterized by a high impedance contrast where a greater amplification in ground motion is expected to occur in case of seismic shaking. If the amplified frequency at a site is close to that of a standing building, a resonance effect may occur and therefore the risk for the building to suffer structural damage greatly increases (*e.g.* Castellaro *et al.* 2014). At this regard, amplification maps are crucial for urban planners in defining the height of buidings (*viz.* the number of floors) characterized by a resonance coincident with the natural one and enabling engineers to improve the antiseismic behaviour of new constructions. Seismic amplification indeed is considered the first cause of damage and collapse during an earthquake.

With the present reasearch we investigated and reconstructed the distribution of the natural amplification due to the occurrence of impedance contrast in the subsoil either in terms of frequency and amplitude of the HVSR (Figures 4 and 5). We focused on the area of Mirandola and surroundings for several reasons. Firstly, because this is a small-medium size industrial district and hence of particular economic and social interest for Italy. As a matter of fact, a second level microzonation investigation has been already commissioned by local authorities and performed before the 2012 Emila earthquake (Tarabusi 2012).

Secondly, the subsoil of the area is characterized by a major growing fault-propagation anticline, where both the causative thrust and the associated fold are completely buried by the Middle-Upper Pleistocene to Holocene continental deposits (*e.g.* Martelli and Molinari 2008; Bonini *et al.* 2014). The differential vertical movements induced by the blind tectonic structure and especially the positive ones (*i.e.* uplift in correspondence of the fold hinge) are not able to keep pace with the regional scale subsidence and the high sedimentation rates of the Po Plain. Therefore, we wanted to test the systematic application of a low-cost geophysical technique in order to gather useful information on the local, relatively shallow, stratigraphy as well as of its seismic behaviour. At this regard, the obtained results clearly and independently document the presence of a folded surface in the shallow Mirandola subsoil; the crest is oriented ESE-WNW with a culmination towards the west and a periclinal setting eastwards in perfect agreement with the tectonic structure reconstructed on the basis of seismic reflection profiles. Accordingly, the results of this methodological approach are quite encouraging and could be easily applied to other morphologically flat regions affected by blind faulting and folding.

Acknowledgements

We are grateful to Luca Martelli for his valuable and helpful suggestions.

References

Bard P.-Y., Acerra C., Alguacil G., Anastasiadis A., Atakan K., Azzara R., Basili R., Bertrand E., Bettig B., Blarel F., Bonnefoy-Claudet S., Bordoni P., Borges A., Bøttger-Sørensen M., Bourjot L., Cara F., Caserta A., Chatelain J-L., Cornou C., Cotton F., Cultrera G., Daminelli R., Dimitriu P., Dunand F., Duval A.-M., Fäh D., Fojtikova L., de Franco R., di Giulio G., Grandison M., Guéguen P., Guillier B., Haghshenas E., Havskov J., Jongmans D., Kind F., Kirsch J., Koehler A., Koller M., Kristek J., Kristekova M., Lacave C., La Rocca M., Marcellini A., Maresca R., Margaris B., Moczo P., Moreno B., Morrone A., Ohrnberger M., Ojeda J.A., Oprsal I., Pagani M., Panou A., Paz C., Querendez E., Rao S., Rey J., Richter G., Rippberger J., Roquette P., Roten D., Rovelli A., Saccoroti G., Savvaidis A., Scherbaum F., Schisselé E., Spühler-Lanz E., Tento A., Teves-Costa P., Theodulidis N., Tvedt E., Utheim T., Vassiliadès J.-F., Vidal S., Viegas G., Vollmer D., Wathelet M., Woessner J., Wolff K. and Zacharapoulos S. (2005) *Guidelines for the implementation of the H/V spectral ratio technique on ambient vibrations measurements, processing and interpretation*. Deliverable D23.12 of the SESAME project, 62 pp, April 2005. Available at http://www.SESAME-FP5.obs.ujf-grenoble.fr

Basili R., Valensise G., Vannoli P., Burrato P., Fracassi U., Mariano S., Tiberti M.M. and Boschi E. (2008) The Database of Individual Seismogenic Sources (DISS), version 3: summarizing 20 years of research on Italy's earthquake geology. *Tectonophys.*, doi:10.1016/j.tecto.2007.04.014

Bigi G., Bonardini G., Catalano R., Cosentino D., Lentini F., Parlotto M. Sartori R., Scandone P. and Turco E. (1992) *Structural model of Italy, 1:500,000*. Consiglio Nazionale delle Ricerche, Rome.

Bignami C., Burrato P., Cannelli V., Chini M., Falcucci E., Ferretti A., Gori S., Kyriakopoulos C., Melini D., Moro M., Novali F., Saroli M., Stramondo S., Valensise G. and Vannoli P. (2012) Coseismic deformation pattern of the Emilia 2012 seismic sequence imaged by Radarsat-1 interferometry. *Annals of Geophys.*, **55**(4), 788-795, doi: 10.4401/ag-6157.

Boccaletti M., Bonini M., Corti G., Gasperini P., Martelli L., Piccardi L., Tanini C. and Vannucci G. (2004) *Seismotectonic Map of the Emilia-Romagna Region, 1:250000*. Regione Emilia-Romagna – CNR.

Bonini L., Toscani G. and Seno S. (2014) Three-dimensional segmentation and different rupture behavior during the 2012 Emilia seismic sequence (Northern Italy). *Tectonophys.*, **630**, 33-42, doi: 10.1016/j.tecto.2014.05.006.

Burrato P., Ciucci F. and Valensise G. (2003) An inventory of river anomalies in the Po Plain, Northern Italy: evidence for active blind thrust faulting. *Ann. Geophys.*, **46**(5), 865-882.

Burrato P., Vannoli P., Fracassi U., Basili R. and Valensise G. (2012) Is blind faulting truly invisible? Tectonic-controlled drainage evolution in the epicentral area of the May 2012, Emilia-Romagna earthquake sequence (northern Italy). *Ann. Geophys.*, **55**(4), 525-531, doi: 10.4401/ag-6182.

Caputo R. (2005) Ground effects of large morphogenic earthquakes. *J. Geodyn.*, **40**(2-3), 113-118.

Caputo R., Pellegrinelli A., Bignami C., Bondesan A., Mantovani A., Stramondo S. and Russo P. (2015) High-precision levelling, DInSAR and geomorphological effects in the Emilia 2012 epicentral area. *Geomorphology*, **235**, 106-117, doi: 10.1016/j.geomorph.2015.02.002

Castellaro S. and Mulargia F. (2009) Vs30 estimates using constrained H/V measurements. *Bull. Seism. Soc. Am.*, **99**, 761-773, doi: 10.1785/0120080179.

Castellaro S., Mulargia F. and Bianconi L. (2005) Passive seismic stratigraphy: a new efficient, fast and economic technique. *J. Geotech. Environ. Geol.*, **3**, 51-77.

Castellaro S., Padròn L.A. and Mulargia F. (2014) The different response of apparently identical structures: a far-field lesson from the Mirandola 20th May 2012 earthquake. *Bull. Earthq. Eng.*, **12** (5), 2481-2493, doi: 10.1007/s10518-013-9505-9.

DISS WORKING GROUP (2015) *Database of Individual Seismogenic Sources (DISS), Version 3.2.0: A compilation of potential sources for earthquakes larger than M 5.5 in Italy and surrounding areas*. http://diss.rm.ingv.it/diss/, © INGV 2015 - Istituto Nazionale di Geofisica e Vulcanologia - All rights reserved, doi: 10.6092/INGV.IT-DISS3.2.0

Gallipoli M.R., Mucciarelli M., Gallicchio S., Tropeano M. and Lizza C. (2004) Horizontal to Vertical Spectral Ratio (HVSR) measurements in the area damaged by the 2002 Molise, Italy, earthquake. *Earthq. Spect.*, **20**(S1), S81-S93, doi: 10.1193/1.1766306.

Gosar A. and Lenart A. (2010) Mapping the thickness of sediments in the Ljubljana Moor basin (Slovenia) using microtremors. *Bull. Earthq. Eng.*, **8**, 501-518, doi: 10.1007/s10518-009-9115-8.

Gruppo di lavoro MS (2008) ICMS, Indirizzi e criteri per la microzonazione sismica. Conferenza delle Regioni e delle Province Autonome - Dipartimento della Protezione Civile, Roma, 3 vol. and Dvd, http://www.protezionecivile.it/cms/view.php?dir_pk=395&cms_pk=15833.

Ibs-von Seht M. and Wohlenberg J. (1999) Microtremor Measurements Used to Map Thickness of Soft Sediments. *Bull. Seism. Soc. Am.*, **89**(1), 250-259.

Koller M., Chatelain J.-L., Guillier B., Duval A.-M., Atakan K., Bard P.-Y. and SESAME Team (2004) Practical user guidelines and software for the implementation of the H/V ratio technique: measuring conditions, processing method and results interpretation. 13th World Conf. Earthq. Eng., Vancouver, August 2004, *Proceedings*, paper # 3132.

Martelli L. and Molinari F.C. (2008) *Studio geologico finalizzato alla ricerca di potenziali serbatoi geotermici nel sottosuolo del comune di Mirandola, Regione Emilia Romagna*. Internal Report, Servizio Geologico, Sismico e dei Suoli, Bologna, pp. 26.

Micromed (2006) *Grilla ver. 2.2, spectral and HVSR analysis – user's manual*. Micromed, Treviso, pp. 47.

Micromed (2008) *An introduction to the phase velocity spectra module in Grilla*. Micromed, Treviso, pp. 16.

Mucciarelli M., Contri P., Mochavesi G., Calvano G. and Gallipoli M.R. (2001) An empirical method to assess the seismic vulnerability of existing buildings using the HVSR technique. *Pure. Appl. Geoph.*, **158**, 2635-2647.

Nakamura Y. (1989) A method for dynamic characteristics estimation of subsurface using microtremor on the ground surface. *Quart. Rep. Railway Tech. Res. Inst.* (RTRI), **30**, 25-33.

Oliveto A.N., Mucciarelli M. and Caputo R. (2004) HVSR prospections in multi-layered environments: an example from the Tyrnavos Basin (Greece). *J. Seismol.*, **8**, 395-406.

Pieri M. and Groppi G. (1981) Subsurface geological structure of the Po Plain, Italy. Consiglio Nazionale delle Ricerche, Progetto finalizzato Geodinamica, sottoprogetto Modello Strutturale, pubbl. N° 414, Roma, 13 pp.

Pondrelli S., Salimbeni S., Perfetti P. and Danecek P. (2012) Quick regional centroid moment tensor solutions for the Emilia 2012 (northern Italy) seismic sequence. *Ann. Geophys.*, **55**(4), 615-621, doi: 10.4401/ag-6146.

Regione Emilia-Romagna (2007) Delibera Assemblea Legislativa n. 112/2007 - Approvazione dell'atto di indirizzo e coordinamento tecnico ai sensi dell'art. 16, comma 1, della LR 20/2000 Disciplina generale sulla tutela del territorio, in merito a "Indirizzi per gli studi di microzonazione sismica in Emilia-Romagna per la pianificazione territoriale ed urbanistica".

Salvi S., Tolomei C., Merryman Boncori J.P., Pezzo G., Atzori S., Antonioli A., Trasatti E., Giuliani R., Zoffoli S. and Coletta A. (2012) Activation of the SIGRIS monitoring system for ground deformation mapping during the Emilia 2012 seismic sequence, using COSMO-SkyMed InSAR data. *Ann. Geophys.*, **55**(4), 796-802, doi: 10.4401/ag-6181.

Saraò A. and Peruzza L. (2012) Fault-plane solutions from moment-tensor inversion and preliminary Coulomb stress analysis for the Emilia Plain. *Ann. Geophys.*, **55**(4), 647-654, doi: 10.4401/ag-6134.

Scognamiglio L., Margheriti L., Mele F.M., Tinti E., Bono A., De Gori P., Lauciani V., Lucente F.P., Mandiello A.G., Marcocci C., Mazza S., Pintore S. and Quintiliani M. (2012) The 2012 Pianura Padana Emiliana seimic sequence: locations, moment tensors and magnitudes. *Ann. Geophys.*, **55**(4), 549-556, doi: 10.4401/ag-6159.

Tarabusi G. (2012) *Microzonazione sismica del comune di Mirandola. Quadro conoscitivo del PSC di Mirandola*. http://www.comune.mirandola.mo.it/la-citta-e-il-territorio/piano-strutturale-comunale-psc, Studio di Geologia Tarabusi, QB_C_REL1, 26/01/2012, Bologna, pp. 57

Vannoli P., Burrato P. and Valensise G. (2015) The seismotectonics of the Po Plain (Northern Italy): tectonic diversity in a blind faulting domain. *Pure Appl. Geophys.*, **172**, 1105-1142, doi: 10.1007/s00024-014-0873-0.

Table 1

Geographic coordinates (latitude and longitude) of the HVSR measurements and the corresponding natural frequency, f_0, and peak value, *A*. Uncertainty on f_0 is commonly around 0.05 with few exception up to 0.15 in case of particularly broad peaks.

label	*lat.*	*lon.*	f_0	*A*
H001	44.8894	11.0702	0.94	2.0
H002	44.8821	11.1963	0.78	2.1
H003	44.8943	11.1793	0.78	2.0
H004	44.8842	11.0714	0.88	2.3
H005	44.8854	11.0782	0.88	2.3
H006	44.8905	11.0819	0.80	2.0
H007	44.8940	11.0686	0.88	2.3
H008	44.8884	11.0634	0.81	2.3
H009	44.8694	11.0610	0.88	3.8
H010	44.8779	11.0552	0.88	3.1
H011	44.8875	11.0527	0.78	2.4
H012	44.8907	11.0341	0.84	2.7
H013	44.8856	11.0433	0.90	2.9
H014	44.8826	11.0639	0.81	2.4
H015	44.8790	11.0631	0.94	2.9
H016	44.8609	11.0595	0.97	4.4
H017	44.8701	11.0482	1.03	3.6
H018	44.8958	11.0878	0.78	2.2
H019	44.8854	11.0670	0.84	2.2
H020	44.8619	11.0623	1.09	4.0
H021	44.8623	11.0564	1.06	4.8
H022	44.8977	11.0708	0.88	2.3
H023	44.9041	11.0649	0.95	2.2
H024	44.8749	11.1277	0.94	2.1
H025	44.8590	11.0441	0.94	2.9
H026	44.8737	11.0094	1.19	3.4
H027	44.8761	11.0194	1.03	3.4
H028	44.8809	11.0484	0.81	3.2
H029	44.9185	11.1025	0.78	2.0
H030	44.9217	11.0911	0.88	2.0
H031	44.9012	11.0688	0.94	2.1
H032	44.8924	11.0752	0.90	2.1
H033	44.8908	11.0597	0.75	2.1
H034	44.8804	11.0554	0.81	3.0
H035	44.8732	11.0454	1.09	3.3
H036	44.8530	11.0374	0.87	2.1
H037	44.8669	11.0560	1.09	3.9
H038	44.8779	11.0751	0.91	2.5
H039	44.8696	11.0651	1.03	4.0
H040	44.8677	11.0641	1.16	4.3
H041	44.8656	11.0693	1.00	4.1
H042	44.8893	11.1014	0.92	1.8
H043	44.8811	11.0263	1.13	3.6
H044	44.8849	11.0285	1.06	3.0
H045	44.8636	11.0194	0.88	2.1
H046	44.9168	11.0654	0.95	2.1
H047	44.8766	11.0906	0.63	2.3
H048	44.8722	11.0807	0.94	2.5
H049	44.8684	11.0760	0.91	3.8
H050	44.8748	11.0683	0.94	2.8
H051	44.8593	11.0563	1.09	3.3
H052	44.8552	11.0511	1.00	2.5
H053	44.8654	11.0265	1.06	2.5
H054	44.8700	11.0281	1.16	2.9
H055	44.8729	11.0001	1.31	2.8
H056	44.8670	11.0098	1.03	2.2
H057	44.8586	11.0279	0.88	2.0
H058	44.8507	11.0459	1.00	1.8
H059	44.8815	11.0694	0.84	2.3
H062	44.8887	11.0573	0.88	2.1
H064	44.8772	11.1332	0.94	1.8
H065	44.8734	11.1015	0.80	2.8
H066	44.8657	11.0959	0.84	3.9
H067	44.8463	11.0888	0.88	2.9
H068	44.8329	11.0770	0.91	2.1
H069	44.8573	11.0927	1.03	4.9
H070	44.8443	11.0701	0.75	2.7
H071	44.8446	11.0560	0.72	2.0
H072	44.8739	11.0345	1.06	4.2

H073	44.8589	11.0882	1.09	4.5
H074	44.8775	11.0629	0.88	3.8
H075	44.8370	11.1589	0.78	2.3
H076	44.8507	11.1733	0.63	2.2
H077	44.8737	11.1861	0.78	2.3
H078	44.8824	11.1614	0.91	2.1
H079	44.8650	11.1522	0.94	2.2
H080	44.8359	11.1379	0.78	2.2
H081	44.8241	11.1000	0.86	1.8
H082	44.8438	11.1069	0.81	2.7
H083	44.8548	11.1107	1.06	3.9
H084	44.8701	11.1200	0.75	2.7
H085	44.8664	11.0818	0.91	4.4
H086	44.8553	11.0748	1.16	3.8
H087	44.8362	11.0637	0.78	2.6
H088	44.8364	11.0536	0.90	2.1
H089	44.8268	11.1622	0.88	1.9
H090	44.8436	11.1697	0.59	2.6
H091	44.8624	11.1779	0.84	2.4
H092	44.8727	11.1547	0.81	2.4
H093	44.8563	11.1505	0.88	2.8
H094	44.8453	11.1453	0.88	3.6
H095	44.8238	11.1323	0.84	2.2
H096	44.8331	11.1056	0.94	2.1
H097	44.8624	11.1139	0.91	3.7
H098	44.8606	11.0772	1.06	5.1
H099	44.8507	11.0712	0.94	3.6
H100	44.9113	10.9943	0.81	2.1
H101	44.8834	10.9884	1.19	4.0
H102	44.8422	10.9564	0.94	1.9
H103	44.8778	10.9653	2.03	4.1
H104	44.8706	10.9751	1.34	4.6
H105	44.8785	10.9910	1.44	3.9
H106	44.9223	11.0320	0.75	1.9
H107	44.8931	11.0111	0.84	2.3
H108	44.8684	11.0028	1.13	3.2
H109	44.8321	11.0316	0.88	2.1
H110	44.9224	10.9955	0.81	2.5
H111	44.8982	10.9902	0.84	2.0
H112	44.8584	10.9670	0.88	2.2
H113	44.8768	10.9839	1.53	4.5
H114	44.8932	10.9985	0.84	2.1
H115	44.8844	11.0070	1.06	3.6
H116	44.8596	11.0000	0.91	1.8
H117	44.8915	11.1109	0.78	2.1
H118	44.9002	11.0763	0.91	2.3
H119	44.8944	11.0591	0.72	2.0
H120	44.8901	11.0956	0.94	2.3
H121	44.8986	11.0816	0.88	2.0
H122	44.9022	11.0594	0.94	2.3
H123	44.8537	11.0691	0.94	4.4
H124	44.8807	11.0769	0.84	2.4
H125	44.8478	11.0620	1.03	1.9
H126	44.9061	10.9703	0.84	2.3
H127	44.9013	10.9618	0.86	2.1
H128	44.8933	10.9729	0.88	2.9
H129	44.8877	10.9636	1.13	3.0
H130	44.8560	10.9552	0.94	1.8
H131	44.8688	10.9556	1.13	3.9
H132	44.8822	10.9570	1.75	3.6
H133	44.8625	10.9850	1.03	2.6
H134	44.8586	11.1254	0.88	3.1
H135	44.8500	11.1347	0.95	2.8
H136	44.8635	11.0609	1.13	5.1

Figure captions

Figure 1: Tectonic sketch map of the buried Northern Apennines fold-and-thrust belt. The box represents the investigated area shown in Figure 2. Modified from Bigi *et al.* (1992).

Figure 2: Map of the investigated area showing the distribution of the HVSR measurements (triangles). A-A' indicate the trace of the seismic reflection profile represented in Figure 6, while *a* to *g* indicate the traces of the profiles shown in Figure 8. Full circles indicate the Mirandola (CH1) and Medolla (CH2) boreholes used for measuring the seismic waves velocity profiles shown in Figure 6, while empty circles the deep bereholes used to interpret section A-A' (corrseponding names are in italics).

Figure 3: Example of HVSR curve (site *H017*) showing the average H/V ratio as a function of the frequency as well as the corresponding standard deviations (thin lines). The arrows emphasise the values considered for the purpose of this paper in terms of the natural frequency, f_0, and maximum amplitude of the ratio (*A*). The shaded areas indicate the disregarded parts of the graph (see text for discussion).

Figure 4: Distribution of the HVSR peak amplitude, *A*, obtained within the investigated area. The darker the color, the higher the value and hence the strongest the impedance contrast. Triangles indicate the measured sites. Corresponding numerical values are also reported in Table 1.

Figure 5: Distribution of the HVSR natural frequency, f_0, obtained within the investigated area. The darker the color, the higher the value and hence the shallower the surface characterized by the impedance contrast. Triangles indicate the measured sites. Corresponding numerical values are also reported in Table 1.

Figure 6: a) HVSR curves obtained from sites investigated within a distance of 200 m from a profile crossing the Mirandola anticline (A-A' in Figure 2). The major peaks in the different graphs have been tentatively correlated along the transect suggesting the possible lateral continuity of the surfaces characterized by some impedance contrast. See for comparison the parallel geological section (b) obtained from a seismic reflection profile and boreholes data (modified from Martelli and Molinari 2008). Legend: 1) Middle-Upper Quaternary continental deposits; 2) Upper Pliocene-Lower Pleistocene marine deposits; 3) Middle Pliocene; 4) Santerno Formation (Lower Pliocene);

5) Porto Garibaldi Formation (Lower Pliocene); 6) Colombacci Formation (Upper Messinian); 7) major thrusts.

Figure 7: 1D velocity profiles obtained at Medolla (a) and Mirandola (b) (see Figure 2 for location) with the crosshole technique (dots). c) and d) the HVSR curves measured at the head site of the two boreholes (black curves) and the modelled ones (gray curves) obtained using the simplified velocity profile shown in (a) and (b) as a stepping black curve.

Figure 8: HVSR curves obtained from sites investigated within a distance of 200 m from the traces *a* to *g* (see Figure 2 for location) crossing the Mirandola anticline. Following the same approach discussed in the text and shown in Figure 6, the major peaks have been tentatively correlated to form a pseudo-2D section.

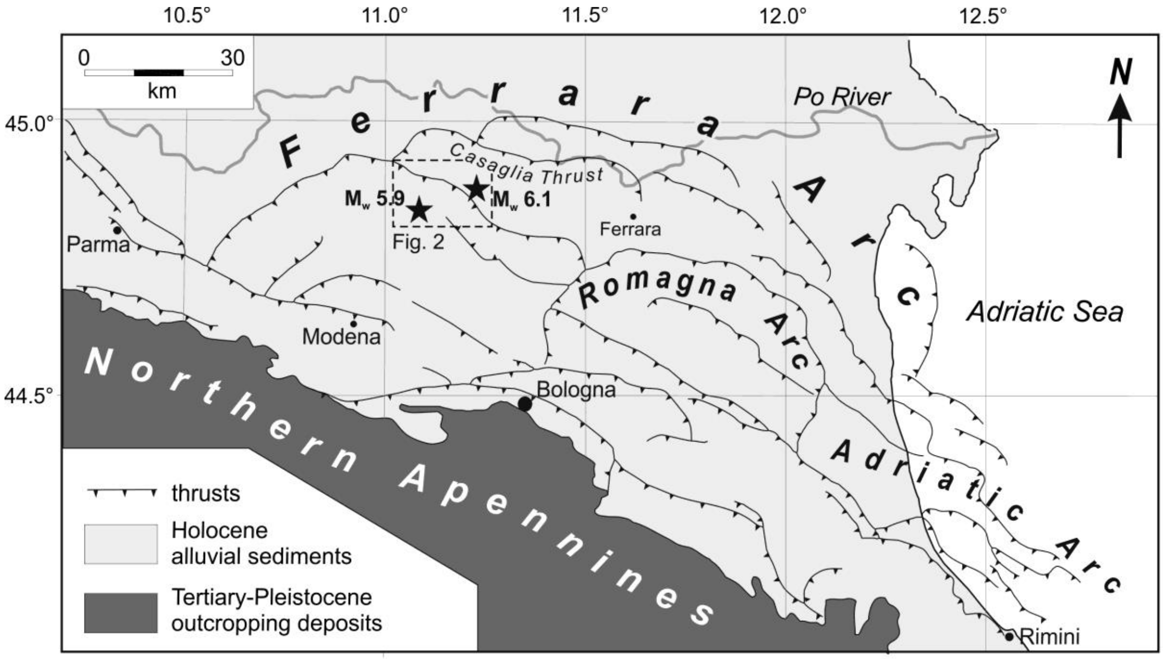

10.5°
11.0°
11.5°
12.0°
12.5°
45.0°
44.5°
0
30
km
N
Po River
Ferrara Arc
Casaglia Thrust
M_w 5.9
M_w 6.1
Fig. 2
Parma
Ferrara
Romagna Arc
Adriatic Sea
Modena
Bologna
Northern Apennines
Adriatic Arc
Rimini
thrusts
Holocene alluvial sediments
Tertiary-Pleistocene outcropping deposits

Figure 1

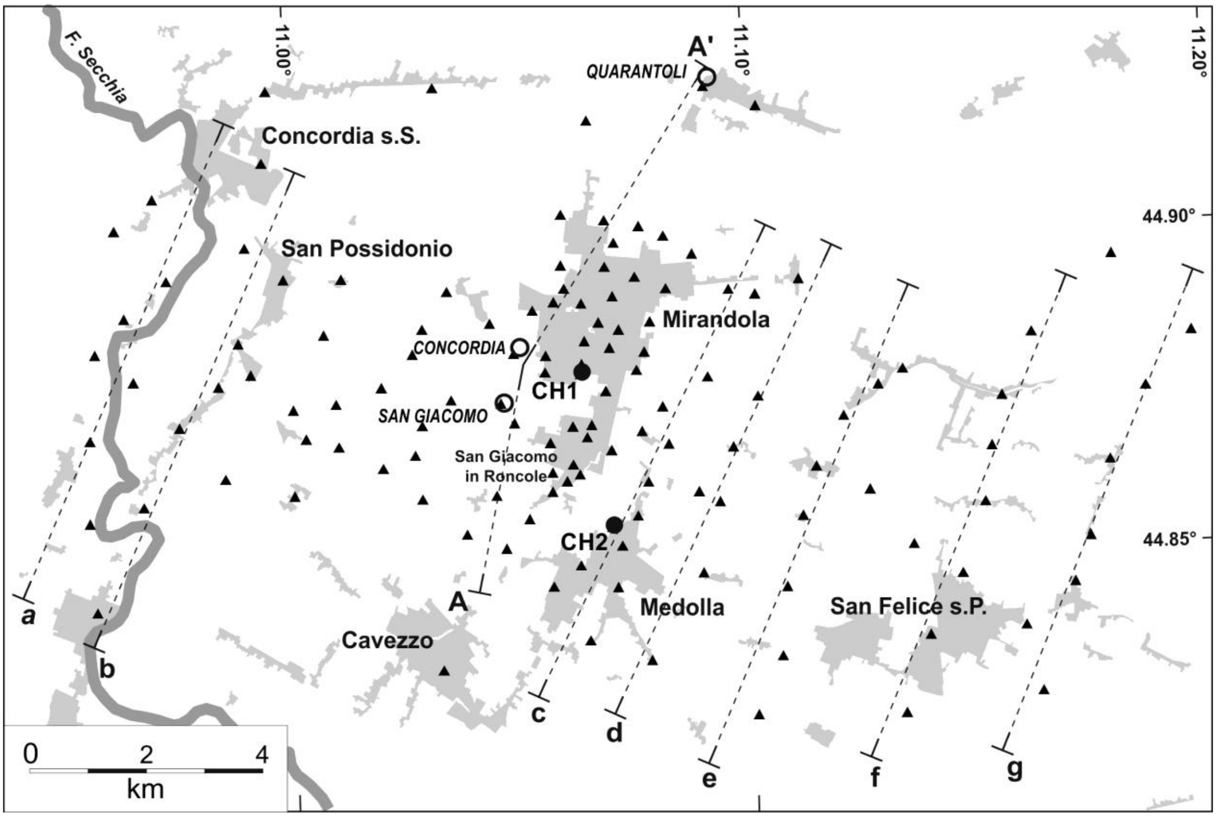
F. Secchia
11.00°
11.10°
11.20°
A'
QUARANTOLI
Concordia s.S.
44.90°
San Possidonio
Mirandola
CONCORDIA
CH1
SAN GIACOMO
San Giacomo
in Roncole
44.85°
CH2
A
a
b
Cavezzo
Medolla
San Felice s.P.
c
d
e
f
g
0
2
4
km

Figura 2

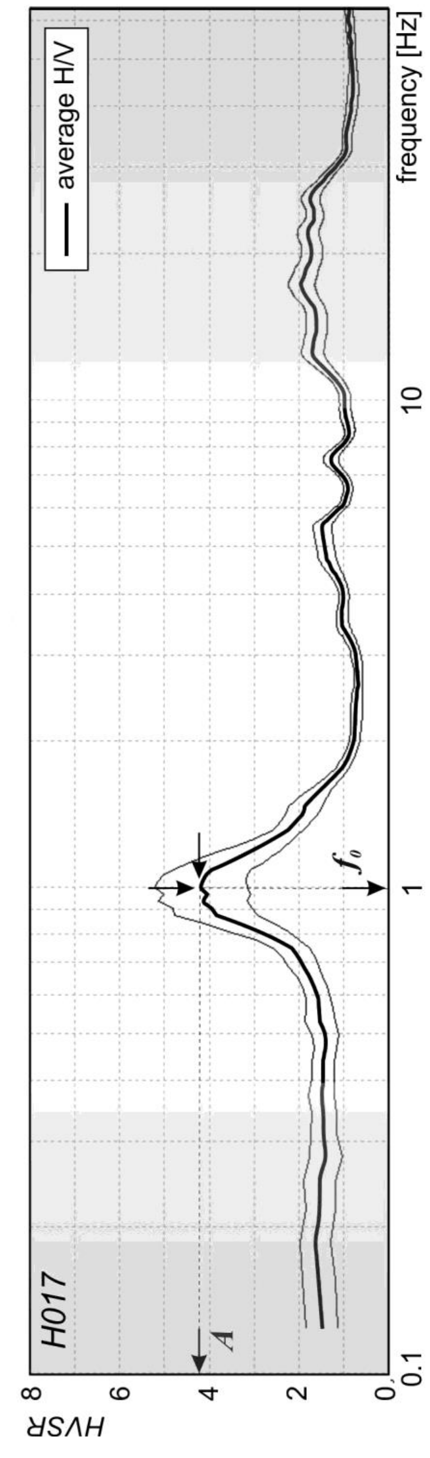

Figure 3

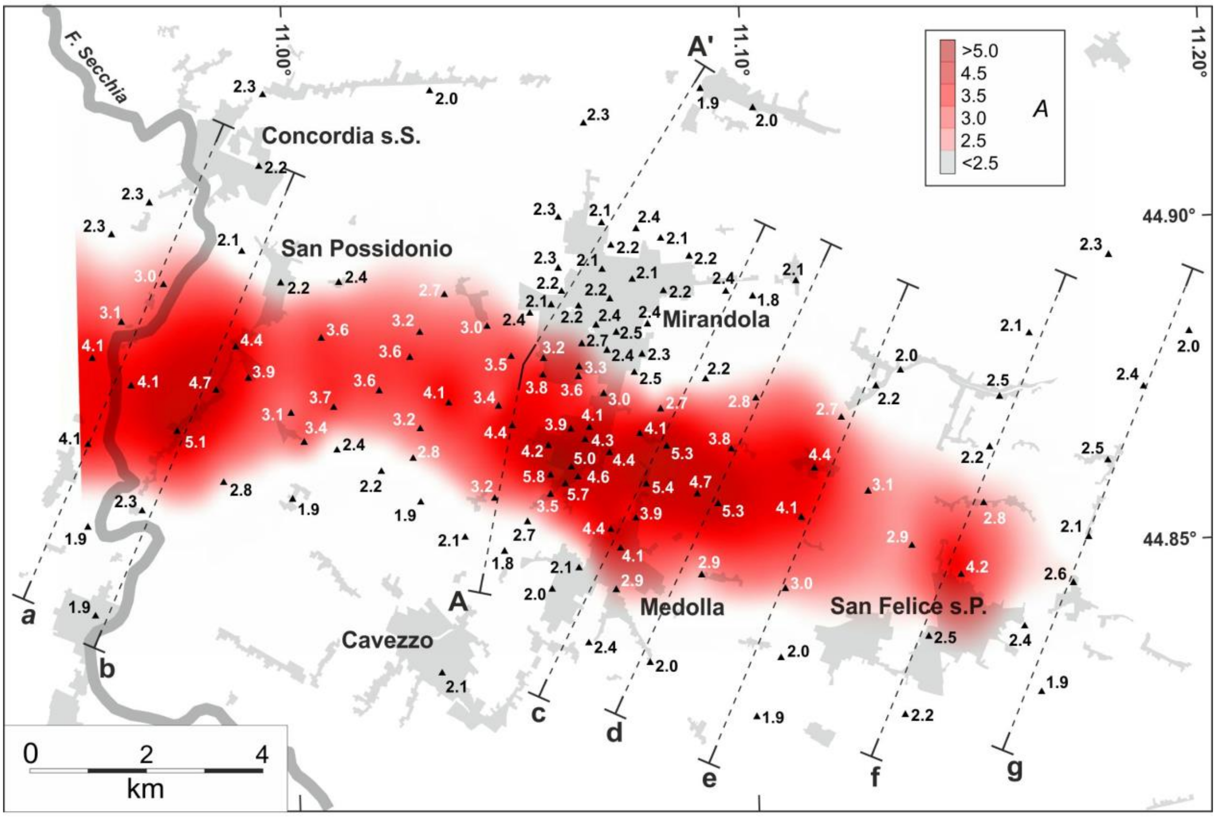

F. Secchia
11.00°
11.10°
11.20°
44.90°
44.85°
A'
A
>5.0
4.5
3.5
3.0
2.5
<2.5
A
Concordia s.S.
San Possidonio
Mirandola
Medolla
San Felice s.P.
Cavezzo
a
b
c
d
e
f
g
0
2
4
km

Figure 4

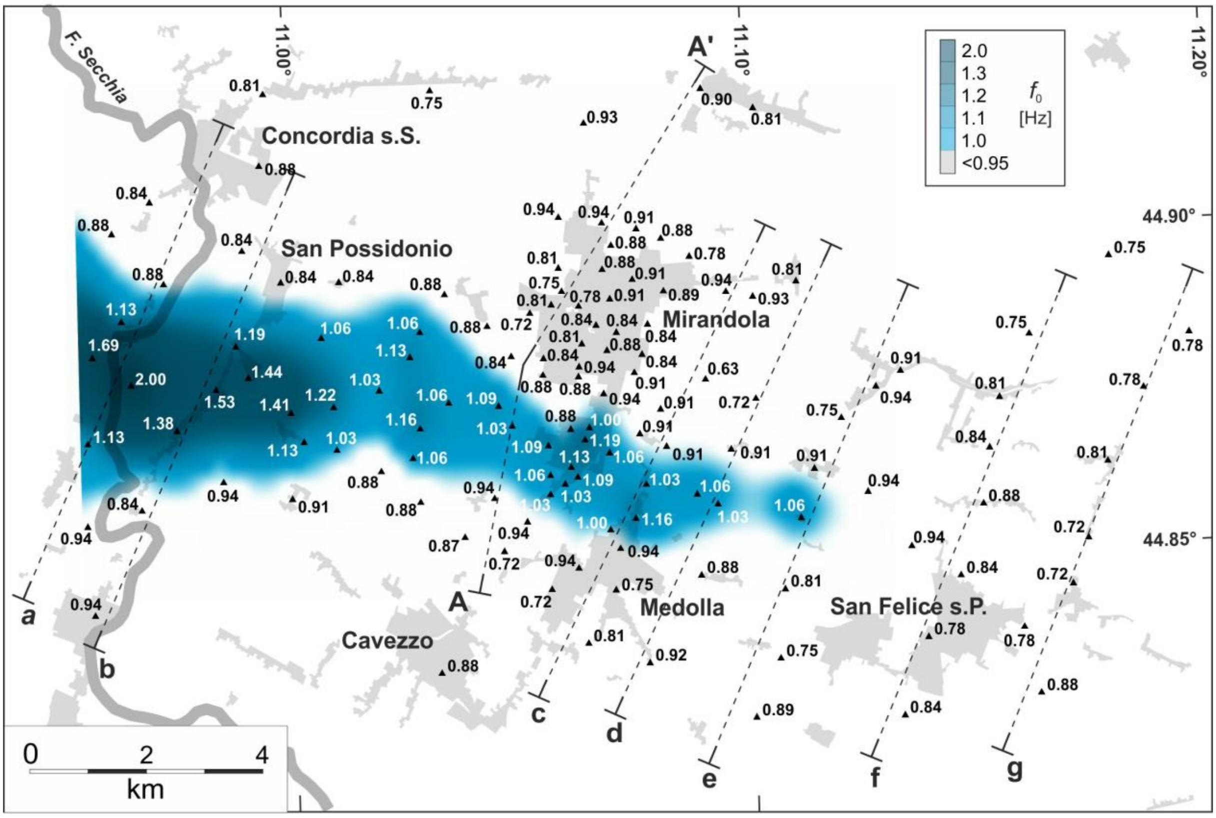
F. Secchia
11.00°
11.10°
11.20°
44.90°
44.85°
Concordia s.S.
San Possidonio
Mirandola
Medolla
Cavezzo
San Felice s.P.
A'
A
a
b
c
d
e
f
g
2.0
1.3
1.2
1.1
1.0
<0.95
f_0
[Hz]
0
2
4
km

Figure 5

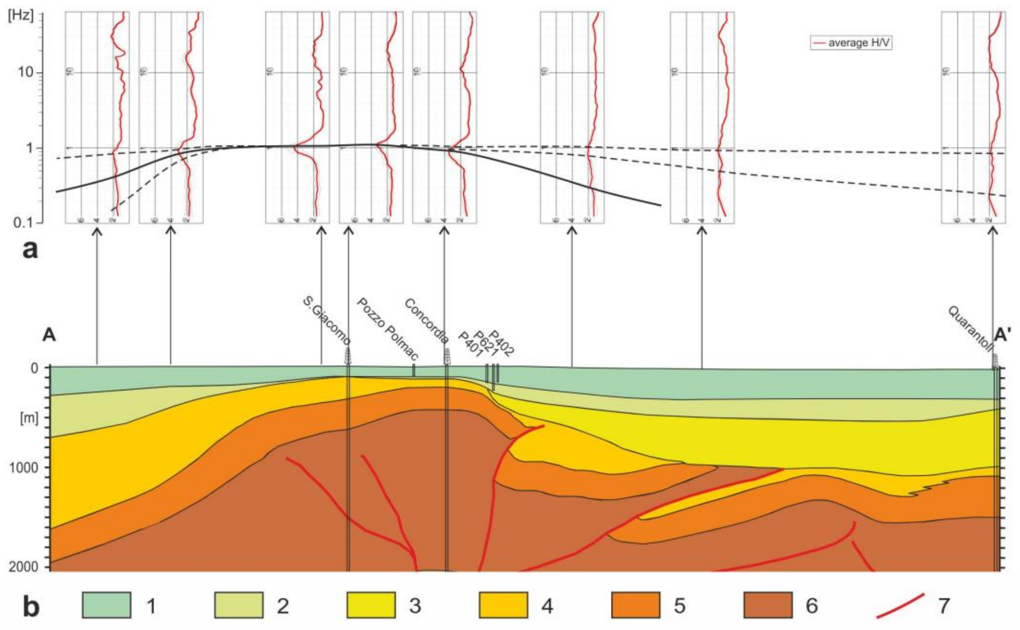
[Hz]
10
1
0.1
average H/V
a
A
A'
S.Giacomo
Pozzo Polmac
Concordia
P401
P621
P402
Quarantoli
0
[m]
1000
2000
b
1
2
3
4
5
6
7

Figure 6

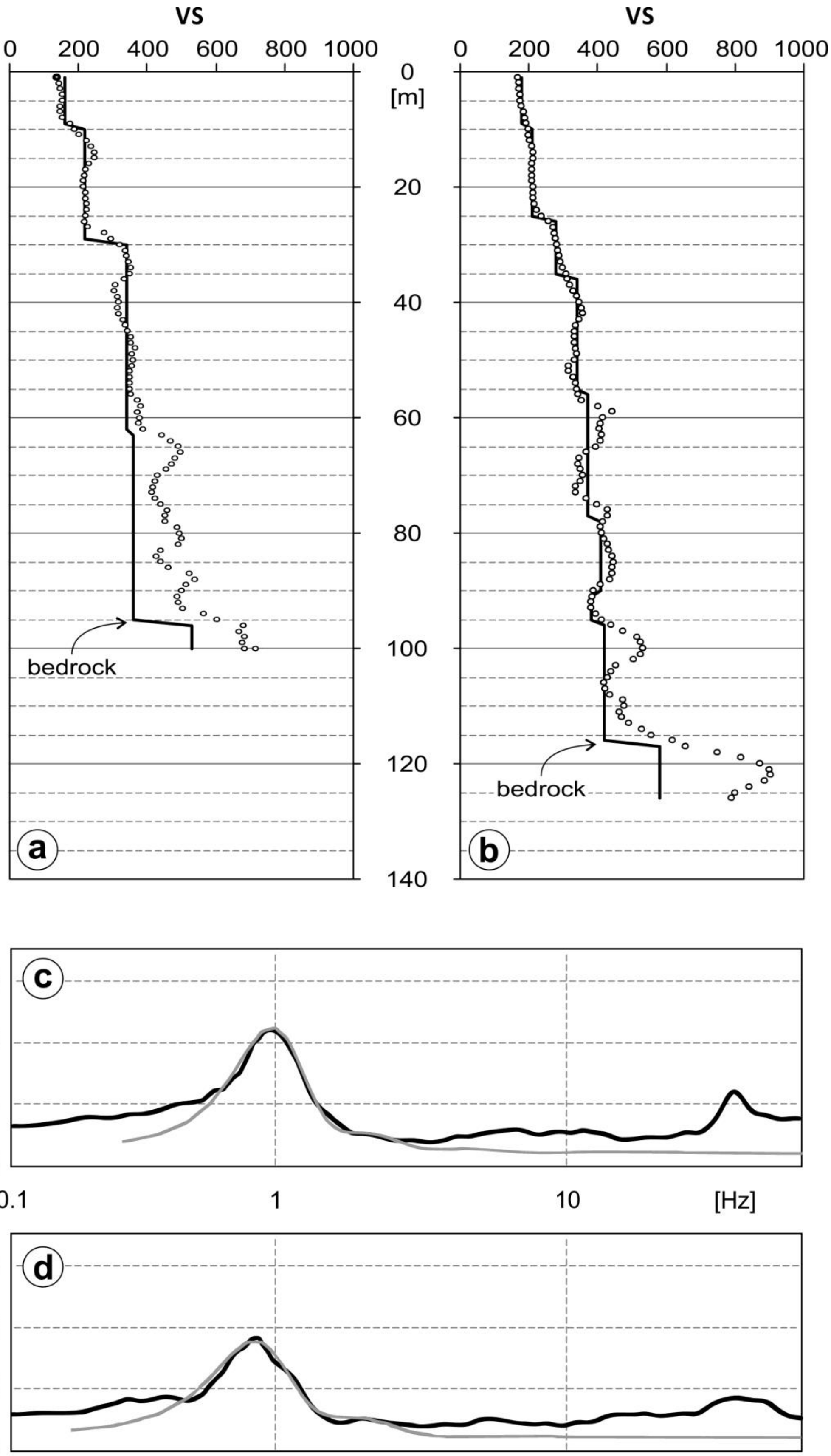
VS
0 200 400 600 800 1000
0
[m]
20
40
60
80
100
120
140
bedrock
a
b
c
d
6
4
2
0
0.1
1
10
[Hz]

Figura 7

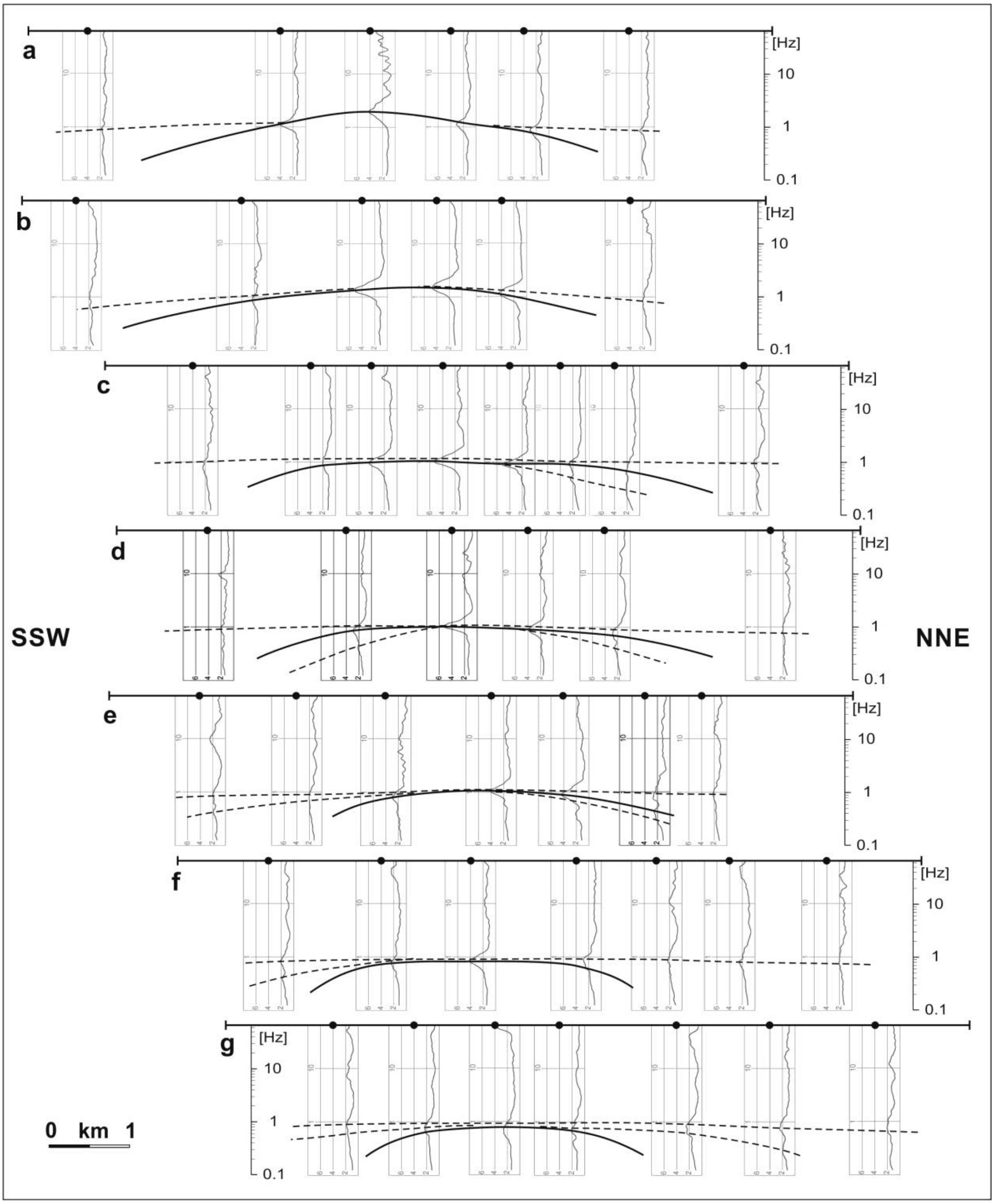

Figure 8